HHS Public Access

Author manuscript

J Cancer Res Ther. Author manuscript; available in PMC 2015 November 13.

Published in final edited form as:

J Cancer Res Ther. 2012 ; 8(4): 565–570. doi:10.4103/0973-1482.106539.

Establishing a framework to implement 4D XCAT Phantom for 4D radiotherapy research

Raj K. Panta[1,2], **Paul Segars**[3], **Fang-Fang Yin**[2], and **Jing Cai**[2]

[1]Department of Medicine, Mannheim, University of Heidelberg, Mannheim, Germany

[2]Department of Radiation Oncology, Duke University Medical Center, Durham, NC, USA

[3]Department of Radiology, Duke University Medical Center, Durham, NC, USA

Abstract

Aims—To establish a framework to implement the 4D integrated extended cardiac torso (XCAT) digital phantom for 4D radiotherapy (RT) research.

Materials and Methods—A computer program was developed to facilitate the characterization and implementation of the 4D XCAT phantom. The program can (1) generate 4D XCAT images with customized parameter files; (2) review 4D XCAT images; (3) generate composite images from 4D XCAT images; (4) track motion of selected region-of-interested (ROI); (5) convert XCAT raw binary images into DICOM format; (6) analyse clinically acquired 4DCT images and real-time position management (RPM) respiratory signal. Motion tracking algorithm was validated by comparing with manual method. Major characteristics of the 4D XCAT phantom were studied.

Results—The comparison between motion tracking and manual measurements of lesion motion trajectory showed a small difference between them (mean difference in motion amplitude: 1.2 mm). The maximum lesion motion decreased nearly linearly (R^2 = 0.97) as its distance to the diaphragm (DD) increased. At any given DD, lesion motion amplitude increased nearly linearly (R^2 range: 0.89 to 0.95) as the inputted diaphragm motion increased. For a given diaphragm motion, the lesion motion is independent of the lesion size at any given DD. The 4D XCAT phantom can closely reproduce irregular breathing profile. The end-to-end test showed that clinically comparable treatment plans can be generated successfully based on 4D XCAT images.

Conclusions—An integrated computer program has been developed to generate, review, analyse, process, and export the 4D XCAT images. A framework has been established to implement the 4D XCAT phantom for 4D RT research.

Keywords

4DCT; lung cancer; motion management; Motion phantom; XCAT

For correspondence: Jing Cai, Department of Radiation Oncology, Duke University Medical Center, Box 3295, Durham, NC 27710, USA. jing.cai@duke.edu.

INTRODUCTION

Motion management is essential to escalate dose to tumor at thorax and abdomen and to minimize unnecessary dose to surrounding healthy tissues. It is recommended that motion management should be considered if tumor motion is greater than 5 mm in any direction or significant normal tissue sparing can be gained.[1] There are widely adopting strategies for motion management in clinics such as motion encompassing, respiratory gating, breath-hold/control, and real-time tumor tracking.[1–7] As new techniques are continuously being developed for managing respiratory motion, it is important to have appropriate tools for validation, evaluation, and selection of these techniques. Motion phantoms of different forms that simulate the mechanical and/or morphological function of the lungs are often used to accomplish the above mentioned tasks. These phantoms typically fall into one of the following three categories: physical phantom, physiological phantom, and digital phantom.

Physical phantoms usually consist of mechanical part like cylindrical insert designed to simulate lung tissue and electrical part that contains a switching power supply and direct current to the adjustable voltage regulatory circuit for driving gear motor with variable velocity.[8] One example of such phantom is the quasar respiratory motion phantom (Modus Medical Devices, Ontario, Canada). The drawback of this type of phantom is that its fabrication is prohibitively expensive for realistic and widely varying geometrical models among patients and it needs frequent operator intervention. The physical phantom involves the motion of physical phantom controlled by a mechanic and an electronic device and has the limitation of limited dimensions and non-deforming simulation.

Physiological phantoms are fabricated to simulate the respiratory motion close to *in vivo* condition which provides easy-to-prepare experimental platform for a variety of imaging studies like 4D-CT/MRI or angiography. The artificial thoracic model of such phantom is characterized by explants of natural specimen like a fresh or plastinated porcin lung, double walled container filled with saline solution to simulate the chest wall and water filled silicon balloon to simulate the diaphragm.[9,10] The lung can be deflated or inflated by a water pump. The lung lesion is simulated by injecting a heated solution of agarose and contrast agent.[9] This type of phantom has been used extensively for monitoring the lung motion, motion of surrogate diaphragm, and the trajectories of artificial lung lesion.[9] This enables to measure anatomical parameters like surrogate diaphragm position, trajectories of lung lesions but the lung motion monitoring method employed here is not applicable directly to human.

Digital phantoms are realistic computer-based simulations of human respiration that provide the virtual model of patient anatomy and physiology. Imaging data can be generated as if it was from real patients using the accurate computerized model of the physics of the imaging process.[11–14] Existing computerized phantoms used in medical imaging involve the trade-off between the realism and flexibility and recent works in digital phantom has focused on creating more hybrid models, phantoms based on patient imaging data, but using more complex mathematical primitives to define the organs and structures. Among there is the 4D digital extended cardio torso (XCAT) phantom which consists of a whole body model that contains the high level anatomical details suitable for application in high resolution imaging

modalities such as CT, MRI, and PET.[12,13] 4D XCAT phantom shares the realism of voxelized phantom and flexibility of mathematical model with whole body anatomies. The respiratory model of 4D XCAT is based on respiratory mechanics and analysis of state of the art respiratory gated CT data which is flexible and parameterized that includes the ability to model the lung nodules of any given size, shape, contrast, and location inside the lungs.[13] The respiratory mechanics of 4D XCAT phantom is controlled by two time curves: diaphragm curve that controls its cranial-caudal (CC) excursion and trajectory, and anterior-posterior (AP) curve that controls its AP excursion and trajectory. 4D XCAT phantom has the flexibility to simulate the respiratory motion of user-defined breathing characteristics.

The objective of this study was to characterize the 4D XCAT digital phantom from the standpoint of 4D radiotherapy (RT) and to establish and validate a clinical workflow of implementing the 4D XCAT phantom for 4D-RT research.

MATERIALS AND METHODS

An integrated computer program was developed in Matlab (R2009a, the Mathworks Inc., Natick, MA) to facilitate the characterization and implementation of the 4D XCAT phantom. Figure 1 shows the workflow of the program that consists of the following essential functions: (1) generating 4D XCAT images, which was achieved by running the core XCAT programs developed by Segars *et al.* All parameters including image modality (CT, MRI, PET, X-ray, etc.), scan volume/resolution, diaphragm motion profile, tumor size/location, etc., were user-defined. Details about the 4D XCAT phantom can be found in the literatures[12,13] and thus will not be repeated here. (2) Reviewing 4D XCAT images, which allows for visualizing the 4D XCAT images in three orthogonal planes (axial, coronal, and sagittal) in a cine loop or at any selected frame. (3) Generating composite images from 4D XCAT, including maximum intensity projection (MIP), average intensity projection (AIP), and minimum intensity projection (MinIP). These composite images can be generated from all frames or user-specified frames. (4) Motion tracking for a selected region of interest (ROI), such as diaphragm, lesion, body surface, etc. The tracking algorithm was based on cross-correlation algorithm and was achieved by firstly defining a rectangular ROI as a template and then searching the maximal cross-correlative region to the template in the following frames. (5) Converting XCAT phantom images from the raw binary format into DICOM format. The output of the XCAT phantom is raw 32 bit floating point binary files with no header (little endian). This binary raw data file was converted into DICOM format which is compatible to Eclipse (Varian Medical Systems, Palo Alto, CA) treatment planning system. The DICOM conversion can be made either to the 4D or 3D XCAT datasets, or the 2D (cine) XCAT images in any selected plane. (6) Analyzing clinically acquired 4DCT and real-time position management (RPM) signal. This function allows extracting useful patient characteristic parameters from 4DCT and RPM for 4D XCAT phantom customization.

All 4D XCAT images used in this study were generated in the attenuation mode (i.e., CT images). Main control parameters were: scan range from neck to mid-abdomen, 120 KeV, 256 × 256 matrix, 2 × 2 × 2 mm^3 spatial resolution. It should be noted that body and lesion were generated separately in two different modes but with the same control parameters. The

final XCAT phantom images were generated by adding these two image datasets afterwards. Prior to the characterization of the 4D XCAT phantom the motion tracking algorithm was firstly validated by comparing the motion trajectory measured using tracking algorithm to that measured manually using ImageJ (U. S. National Institutes of Health, Bethesda, Maryland, USA).

Major characteristics of the 4D XCAT phantom that are relevant to 4D RT applications were studied as described below: (1) Dependence of lesion motion on lesion location. Using the diaphragm position in the end-of-exhalation phase as a reference, the CC location of the lesion was indicated by the distance between the lesion center to the distal end of the diaphragm (DD), as shown in Figure 2. 4D XCAT images were generated with the same body anatomy but with lesions at different CC locations (DD = 7.2, 9.6, 11.2, 13.4, and 15.4 cm, respectively). The AP and medial-lateral (ML) locations of the lesion were close to the center of the ipsilateral lung and were kept the same. (2) Dependence of lesion motion on diaphragm motion. Lesion motion trajectories were determined with different maximum diaphragm excursion of 20, 30, 40, and 50 mm, and at different DDs of 9.0, 13.4, and 15.4 cm. (3) Dependence of lesion motion on lesion size. Lesion motion trajectories were measured with different lesion diameter of 20, 30, 40, and 50 mm, and at different DDs of 9.0 and 15.4 cm. (4) Customization of phantom motion. A real patient's RPM data were inputted as the diaphragm profile for XCAT generation. Measured diaphragm motion from the XCAT images were then compared to the inputted RPM signal.

End-to-end test of the implementation of the 4D XCAT was performed. In this example, ten frames were generated over a whole respiratory cycle. MIP and AIP images were generated using all ten frames, converted to DICOM format, and imported into Eclipse treatment planning system for contouring and planning. Internal target volume (ITV) was delineated in the MIP, and organs at risk (OARs) including lung, heart, spinal cord, chest wall, etc., were delineated in the AIP. Planning target volume (PTV) was created by adding a 5 mm margin to the ITV. A lung SBRT plan was created on the AIP using co-planar 3D conformal technique. The prescription dose of 48 Gy in four fractions was designed to provide coverage for 95% of PTV. Dose constraints to OARs were adapted from radiation therapy oncology group (RTOG) 0915 protocol. Analytical anisotropic algorithm (AAA) was used for dose calculation.

RESULTS

The comparison between automatic and manual measurements [Figure 3] showed a small difference between the two (mean difference in motion amplitude: 1.2 mm), indicating that the cross-correlation based tracking algorithm is a reliable method for motion measurement in this study.

Figure 4 shows the CC motion trajectories of the lesion measured at different DDs, along with the motion trajectory of the diaphragm. It can be seen that the motion amplitude of the lesion decreases as the DD increases (or as the lesion sites more superiorly in the lungs). It can also be seen that the peaks of all motion trajectories occur at the same frame (or at the same respiratory phase), indicating that there is no phase shift of lesion's motion at different

lesion locations. Furthermore, as shown in Figure 5, the maximum lesion motion decreased nearly linearly (R^2 = 0.97) as the DD increased.

Figure 6 shows the correlation between the lesion motion and the inputted diaphragm motion. At any given DD, lesion motion amplitude increased nearly linearly (R^2 range: 0.89 to 0.95) as the inputted diaphragm motion increased. For a given diaphragm motion, the lesion motion is independent of the lesion size at any given DD [Figure 7]. Figure 8 shows that the 4D XCAT phantom can closely reproduce irregular breathing profile: the mean difference in motion amplitude between the inputted and the measured motion profile was 1.4 mm.

Figure 9 shows example MIP, AIP, and MinIP images that were generated from the 4D XCAT. Figure 10 shows the beam arrangement and dose distribution of the lung SBRT plan created on the XCAT phantom. With 95% of PTV receiving 48 Gy, V20 for the lungs was 6.7%, max cord dose was 17.4 Gy, and comformality index was 1.15. These results are comparable to clinical plans of real patients.

DISCUSSION

It is a consensus that adequate knowledge of tumor and organ respiratory motion is important and should be acquired prior to treatment planning in order to assure adequate dose to the target and to avoid unnecessary dose to normal tissues during radiation therapy for cancers in the thorax and abdomen. It is still unclear, however, how such knowledge can be best used to benefit the patient the most. The latest breakthrough in the advancement of computer based digital phantom, such as the 4D XCAT phantom, is of great importance in answering this question since these phantoms can be used to test, validate, and quality assure different strategies of motion management on the individual patient basis. In this study, we explored the feasibility of implementing the 4D XCAT phantom for 4D RT research by characterizing its major characteristics from the standpoint of tumor motion management, and by establishing a robust workflow for its implementation. The study on the characterizations of the 4D XCAT phantom showed that the motion of the lesion highly dependent upon its position and the inputted motion profile of the diaphragm, but independent of its size. As expected, the motion of the lesion is greater when it is closer to the diaphragm. The greater the inputted motion of the diaphragm is, thegreater is the motion of the lesion. These observed motion characteristics of the lesion are close approximations of real patients' respiratory mechanics. The end-to-end test showed that we have successfully established a robust workflow to generate, review, analyze, process, and export the 4D XCAT images for treatment planning.

Several potential limitations of the 4D XCAT phantom were observed in this study. (1) The tissues in XCAT phantom are modeled homogenously, i.e., same CT number is assigned to the same organ or sub-organ. This is a clear deviation from real patients as pointed by the developers.[12,13] The dosimetric impact of such deviation is to be investigated. (2) The comparison of lesion trajectories at different DDs showed that there is no phase shift effect. The average 3D trajectory of the lung lesion in human shows hysteresis-like behavior, i.e., the lesion follows a path during inhalation that is different from that during exhalation.[15]

Such effect was not observed in the 4D XCAT phantom. (3) Motion of the lesion cannot be independently controlled. Motion of the lesion is controlled by its location and the inputted diaphragm motion in the 4D XCAT phantom. However, many studies have shown that tumor at same location can move considerably differently between patients, and could have weak correlation with the diaphragm motion.[16] (4) Shape of the lesion cannot be easily modified. Though different parameters such as size and location of lesion are provided in the XCAT program file to define the lesion in the body, it is basically modeled as simple sphere only and any alternation in the shape of lesion needs original software intervention by modelling the lesion with 3D non-uniform rational B-spline (NURBS).

It was demonstrated in this study that the motion pattern of 4D XCAT phantom can be individually customized to simulate even complex and irregular respiratory motion. In addition, the anatomy of 4D XCAT phantom can be customized to best approximate a real patient's anatomy. The high flexibility of 4D XCAT phantom makes it a potential patient-specific 4D quality assurance (QA) tool. Current XCAT phantom requires manual input to define anatomical parameters in order to customize the phantom, which is labor-intensive and impractical for clinical applications. Future studies on automating the customization with the aid of advanced image techniques such as deformable image registration is therefore highly desirable. In addition, the 4D XCAT phantom can also be used in 4D imaging research to test and validate novel imaging techniques. Although not shown in this study, we have created simulation tools of 4DCT and 4DMRI based on the 4D XCAT phantom. An example for the development of 4D-MRI can be seen in the literature.[17]

CONCLUSION

An integrated computer program has been developed to generate, review, analyze, process, and export the 4D XCAT images for 4D RT research. Major characteristics of the 4D XCAT phantom have been studied and an end-to-end test from XCAT image generation to treatment planning has been successfully performed. These preliminary results demonstrated that we have established a robust workflow to implement the 4D XCAT phantom for 4D RT research.

References

1. Keall PJ, Mageras GS, Balter JM, Emery RS, Forster KM, Jiang SB, et al. The management of respiratory motion in radiation oncology report of AAPM Task Group 76. Med Phys. 2006; 33:3874–900. [PubMed: 17089851]
2. Kitamura K, Shirato H, Seppenwoolde Y, Onimaru R, Oda M, Fujita K, et al. Three-dimensional intrafractional movement of prostate measured during real-time tumor-tracking radiotherapy in supine and prone treatment positions. Int J Radiat Oncol Biol Phys. 2002; 53:1117–23. [PubMed: 12128110]
3. Lujan AE, Larsen EW, Balter JM, Ten Haken RK. A method for incorporating organ motion due to breathing into 3D dose calculations. Med Phys. 1999; 26:715–20. [PubMed: 10360531]
4. McNair HA, Brock J, Symonds-Tayler JR, Ashley S, Eagle S, Evans PM, et al. Feasibility of the use of the Active Breathing Coordinator (ABC) in patients receiving radical radiotherapy for non-small cell lung cancer (NSCLC). Radiother Oncol. 2009; 3:424–9. [PubMed: 19854526]
5. Sakakibara-Konishi J, Oizumi S, Kinoshita I, Shinagawa N, Kikuchi J, Kato M, et al. Phase I study of concurrent real-time tumor-tracking thoracic radiation therapy with paclitaxel and carboplatin in locally advanced non-small cell lung cancer. Lung Cancer. 2011; 74:248–52. [PubMed: 21397973]

6. Saw CB, Brandner E, Selvraj R, Chen H, Saiful Huq M, Heron DE. A review on clinical implementation of respiratory-gated radiation therapy. Biomed Imaging Interv J. 2007; 3:e40. [PubMed: 21614265]
7. Tahir BA, Bragg CM, Lawless SE, Hatton MQ, Ireland RH. Dosimetric evaluation of inspiration and expiration breath-hold for intensity-modulated radiotherapy planning of non-small cell lung cancer. Phys Med Biol. 2010; 55:N191–9. [PubMed: 20348604]
8. Fitzpatrick MJ, Starkschall G, Balter P, Antolak JA, Guerrero T, Nelson C, et al. A novel platform simulating irregular motion to enhance assessment of respiration-correlated radiation therapy procedures. J Appl Clin Med Phys. 2005; 6:13–21. [PubMed: 15770194]
9. Remmert G, Biedere J, Lohberger F, Fabel M, Hartmann GH. Four-dimensional magnetic resonance imaging for the determination of tumour movement and its evaluation using dynamic porcine lung phantom. Phys Med Biol. 2007; 52:N401–15. [PubMed: 17804874]
10. Yoon S, Henry RW, Bouley DM, Bennett NR, Fahrig R. Characterisation of a novel anthropomorphic plastinated lung phantom. Med Phys. 2008; 35:5934–43. [PubMed: 19175148]
11. Lee C, Lodwick D, Hasenauer D, Williams JL, Lee C, Bolch WE. Hybrid computational phantoms of the male and female newborn patient: NURBS-based whole-body models. Phys Med Biol. 2007; 52:3309–33. [PubMed: 17664546]
12. Segars WP, Mahesh M, Beck TJ, Frey EC, Tsu BM. Realistic CT simulation using the 4D XCAT phantom. Med Phys. 2008; 35:3800–8. [PubMed: 18777939]
13. Segars WP, Sturgeon G, Mendonca S, Grimes J, Tsui BM. 4D XCAT phantom for multimodality imaging research. Med Phys. 2010; 37:4902–15. [PubMed: 20964209]
14. Zubal IG, Harrell CR, Smith EO, Rattner Z, Gindi G, Hoffer PB. Computerized three-dimensional segmented human anatomy. Med Phys. 1994; 21:299–302. [PubMed: 8177164]
15. Shirato H, Seppenwoolde Y, Kitamura K, Onimura R, Shimizu S. Intrafractional tumour motion: Lung and liver. Semin Radiat Oncol. 2004; 14:10–8. [PubMed: 14752729]
16. Stevens CW, Munden RF, Forster KM, Kelly JF, Liao Z, Starkschall G, et al. Respiratory-driven lung tumor motion is independent of tumor size, tumor location, and pulmonary function. Int J Radiat Oncol Biol Phys. 2001; 51:62–8. [PubMed: 11516852]
17. Cai J, Chang Z, Wang Z, Paul Segars W, Yin FF. Four-dimensional Magnetic Resonance Imaging (4D-MRI) using image-based respiratory Ssrrogate: A feasibility Study. Med Phys. 2011; 38:6384–94. [PubMed: 22149822]

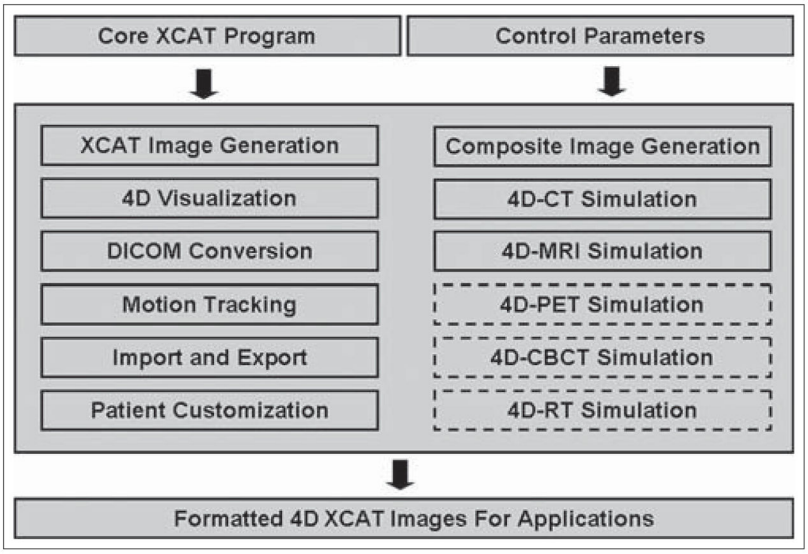

Figure 1.

Workflow of the integrated computer program. Functions in solid boxes have been implemented in the program. Functions in dashed boxes are to be implemented

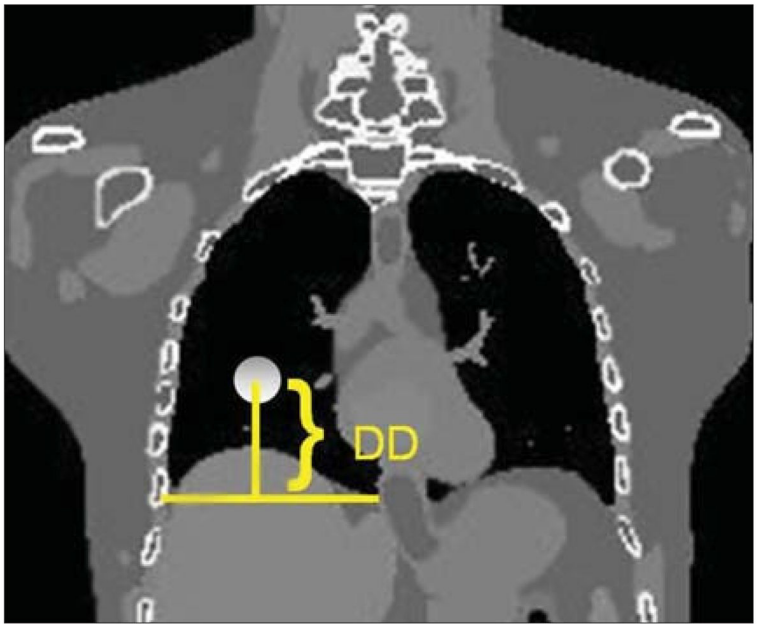

Figure 2.
Defination of DD: distance between the center of the lesion to the distal end of the diaphragm

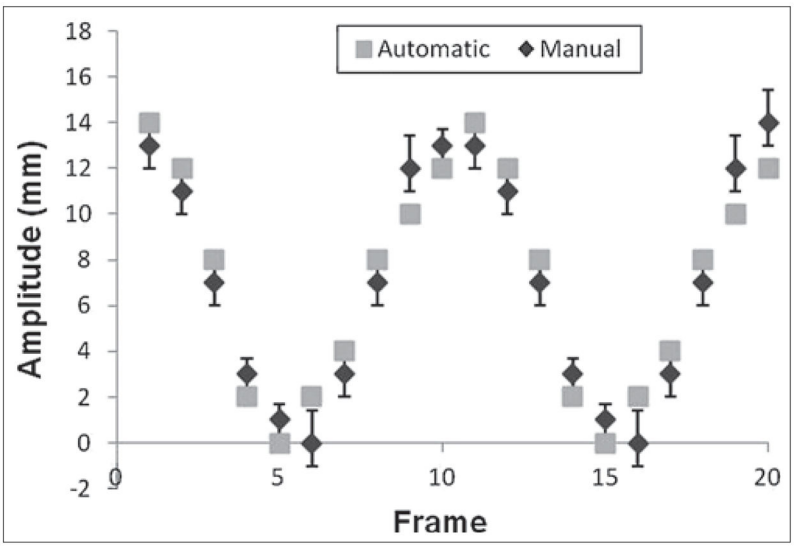

Figure 3.
Comparision of motion trajectories measured using the motion tracking method and the manual method

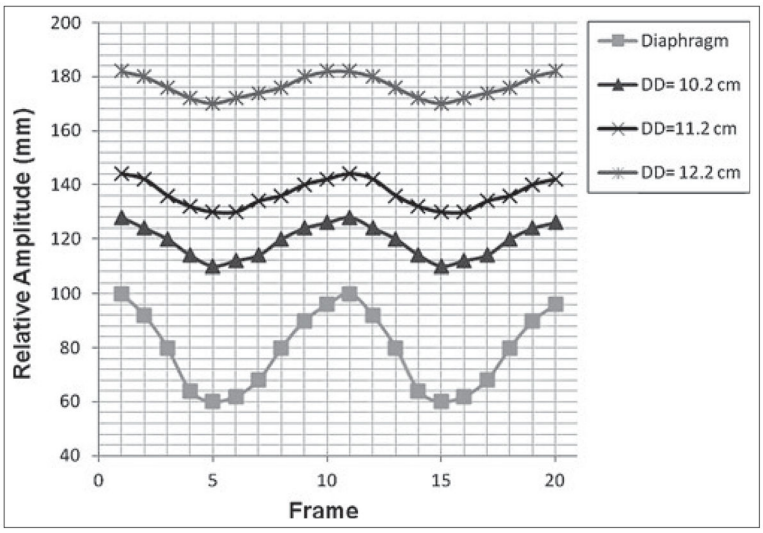

Figure 4.
Cranial-caudal motion trajectories of the lesion at different DDs and of the diaphragm

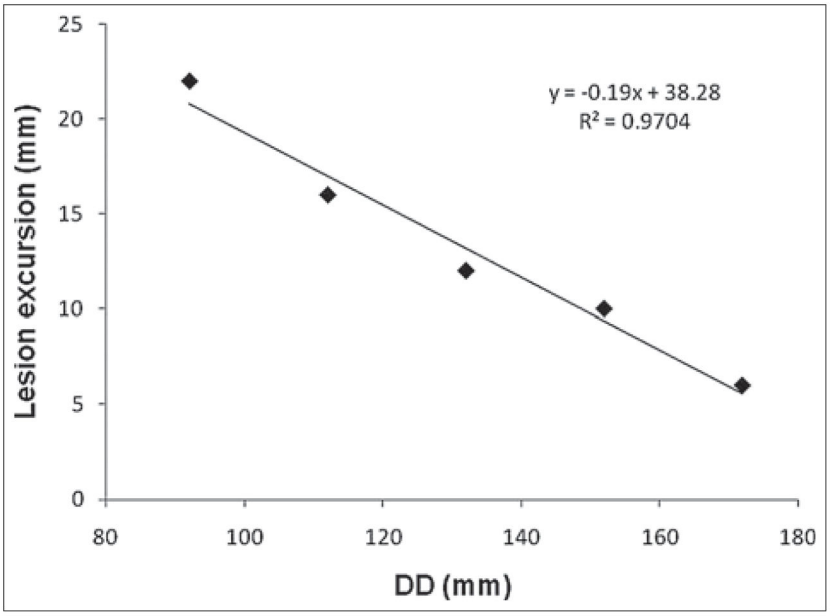

Figure 5.
Dependency of maximum cranial-caudal motion of the lesion on DD

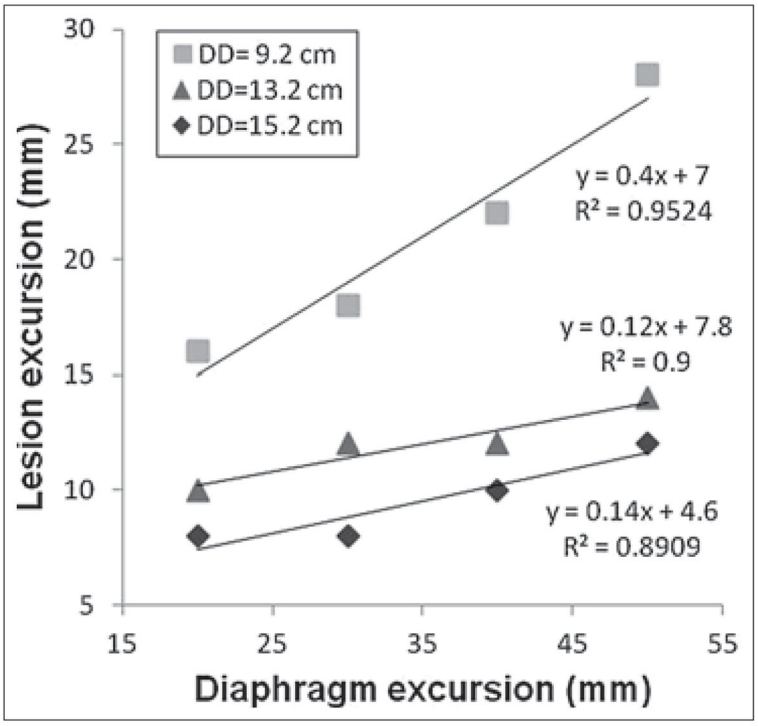

Figure 6.

Dependency of maximum cranial-caudal motion of the lesion on the motion magnitude of disphram at different DDs

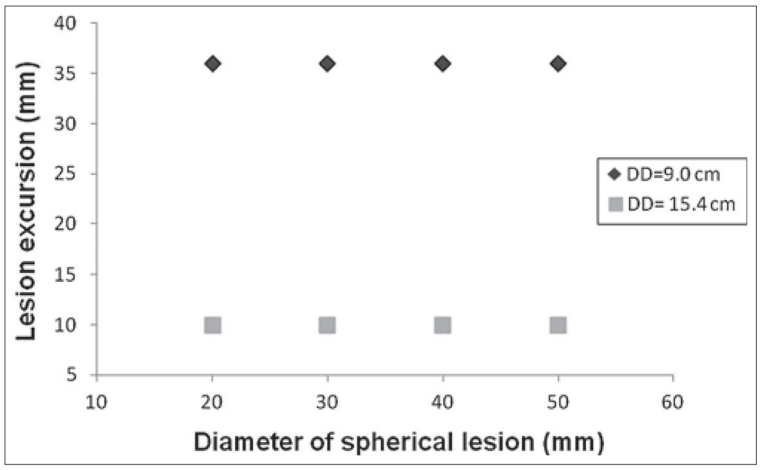

Figure 7.

Dependency of maximum cranial-caudal motion of the lesion on the size of the lesion at different DDs

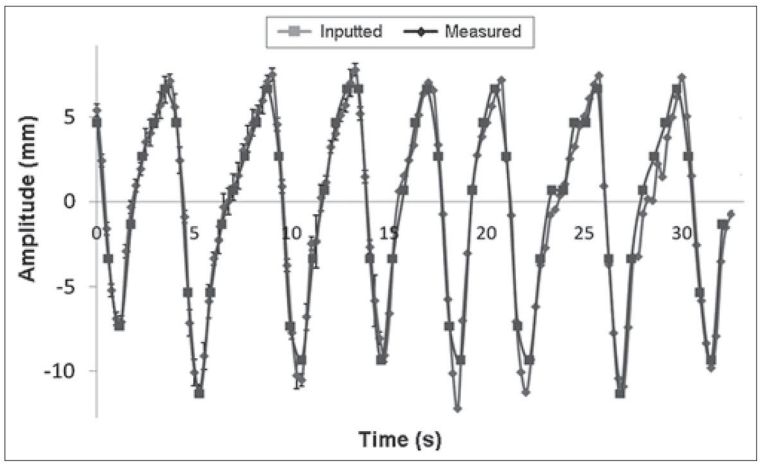

Figure 8.
Comparision between the measued and the inputted motion trajectories

Figure 9.
Example of composite images of MIP (top), AIP (middle), and MinIP (bottom)

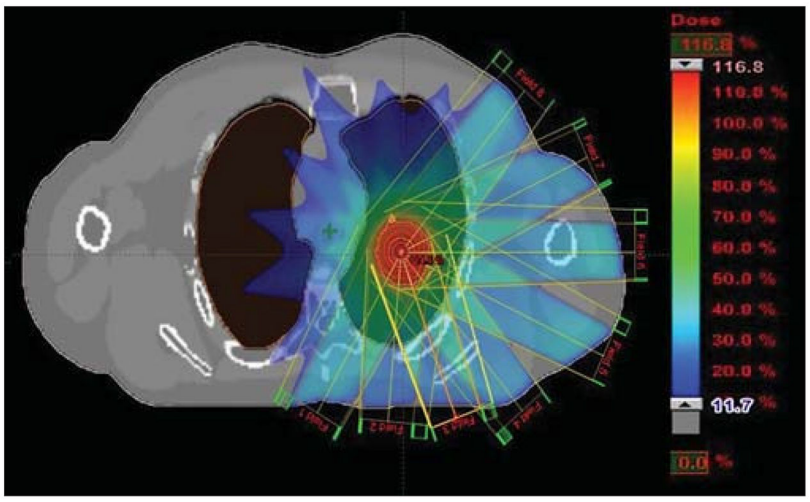

Figure 10.
Beam arrangement and dose distribution of a lung SBRT plan created on the XCAT phantom